

Ultrahigh-Throughput Enrichment of Circulating Tumor Cells from Whole Blood

Yingchao Meng,[#] Mahmut Kamil Aslan,[#] Qingmei Xu, Sarah Duclos Ivetich, Yanan Zhang, Alexander Ring, Tobias Weiss, Stavros Stavrakis,^{*} and Andrew J. deMello^{*}



Cite This: <https://doi.org/10.1021/acssensors.5c04510>



Read Online

ACCESS |



Metrics & More



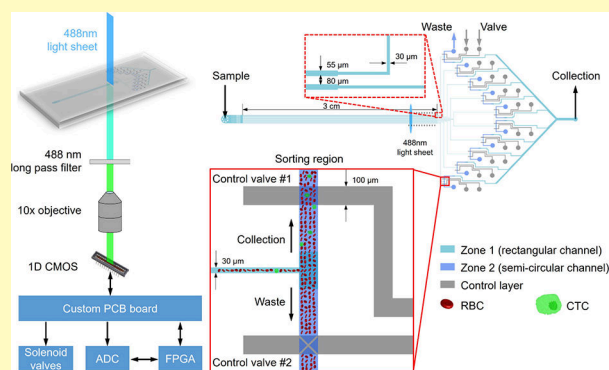
Article Recommendations



Supporting Information

ABSTRACT: Circulating tumor cells (CTCs) in peripheral blood serve as valuable indicators of cancer progression and important biomarkers for the early diagnosis and prognosis of the disease. Unfortunately, CTCs are typically present at extremely low concentrations, and the challenge of enriching and isolating rare cells is often insurmountable. Herein, we present a fluorescence-based active cell sorting system designed to isolate rare cells from peripheral blood. Our platform is based on the principle of positive selection, where cell-surface markers are specifically labelled with fluorescent antibodies, ranked by aliquots, and subsequently sorted. The developed system comprises a multilayer microfluidic device that incorporates 10 parallel channels equipped with pneumatically actuated control valves. A one-dimensional complementary metal-oxide-semiconductor image sensor integrated with a field-programmable gate array enables real-time fluorescence detection across all channels, with the system processing 0.5 mL of minimally processed whole blood per minute. The platform is validated by spiking cancer cells into 5-fold diluted, minimally processed whole blood, at a ratio of $1:10^8$ cancer cells to blood cells. Remarkably, after only three rounds of sorting, cancer cells are enriched by 8 orders of magnitude with a recovery rate exceeding 90%. To showcase the utility of the platform as a clinical tool, we assay clinical blood samples from cancer patients, successfully isolating CTCs at an average concentration of 7.6 CTCs/mL. Such performance metrics confirm immediate utility in the enrichment of CTCs and as a minimally invasive biopsy tool in clinical diagnostics and cancer research.

KEYWORDS: circulating tumor cells, fluorescence-based active cell sorting system, fluorescent antibodies, ensemble-decision aliquot ranking, cancer cells



More than 90% of cancer-related deaths are caused by cancer metastasis, primarily driven by the dissemination of circulating tumor cells (CTCs) through the bloodstream.^{1,2} The metastatic process occurs as cancer cells detach from their primary or metastatic sites and enter the peripheral blood. Subsequently, these hold the potential to infiltrate and establish secondary tumors at distant locations. Studies have demonstrated that the number of CTCs is closely related to cancer progression and metastasis,³ making it a valuable predictive marker that can in principle be analysed through minimally invasive liquid biopsy methods.^{4,5} Unfortunately, the detection and analysis of CTCs is enormously challenging due to their extremely low abundance in comparison to other blood constituents, with CTCs being present in quantities between 1 and 100 cells per mL of blood.^{6–9}

Conventional CTC separation techniques rely on identifying differences between the (biological or physical) characteristics of CTCs (1–100 cells/mL) and more abundant red blood (RBCs, ~ 5 billion/mL of blood) and white blood cells (WBCs, ~ 7 million/mL of blood).¹⁰ The biological properties of CTCs are normally characterized through the expression of specific

epithelial surface markers, such as EpCAM, EGFR, HER2, and MUC1, while properties such as size, shape, deformability, density, and relative permittivity can be used to assess physical and mechanical attributes.^{11,12} That said, it is important to note that CTCs exhibit significant time-dependent heterogeneity in both physical and biological attributes, making identification non-trivial.¹³

In recent years, microfluidic-based cell sorters have emerged as promising tools for separating and enriching CTCs.¹⁴ Such systems offer several advantages over conventional approaches, including improved separation efficiency and recovery, biocompatibility, and cost-effectiveness. Microfluidic cell sorters designed for the enrichment of CTCs can be classified according to the method of

Received: November 27, 2025

Revised: February 20, 2026

Accepted: March 16, 2026

enrichment, with physical-based enrichment methods leveraging variations in the physical and mechanical properties of cells (such as size and deformability) and immunoaffinity-based enrichment methods depending on the expression of specific surface markers.^{15,16} Among physical-based enrichment techniques, inertial microfluidic systems are particularly appealing as they are able to process samples at mL/min volumetric flow rates.^{17–20} While size-based separation methods are attractive by virtue of their simplicity and “label free” nature, their widespread utility in CTC isolation is limited by the fact that CTC size distributions overlap significantly with the size distributions associated with white blood cells.¹⁶ This means that techniques able to capture small CTCs will also capture large WBCs, compromising the accuracy of downstream molecular analyses and hampering the study of individual CTCs.^{11,17,21} In contrast, immunoaffinity-based separation methods, which rely on the identification of epithelial surface markers, provide for more specific enrichment of CTCs.^{11,15,22,23} Currently, the *CellSearch* system, introduced by Janssen Diagnostics in 2004, is the only immunoaffinity-based CTC enrichment and detection system approved by the US Food and Drug Administration for use in clinical applications, and thus serves as the current ‘gold standard’ method for CTC isolation. This method is based on immunomagnetic separation, employing ferrofluid particles coated with antibodies to target EpCAM. Subsequently, isolated cells are immunostained with fluorescently labelled antibodies and imaged. While the *CellSearch* system has demonstrated real prognostic utility,²⁴ several studies have identified important limitations in regard to sensitivity and its ability to detect CTCs in metastatic patients. Of particular concern is an inability to detect CTCs with low EpCAM expression.^{25,26} Additionally, tumor cells with low EpCAM expression often exhibit more mesenchymal characteristics, which are associated with enhanced cancer progression and metastatic potential.^{25,27} In such cases, the *CellSearch* system exhibits low recovery rates, e.g., 2% for mesenchymal breast cancer cell lines.²⁸ Moreover, the *CellSearch* system typically isolates CTCs in the presence of a high background of contaminating WBCs, resulting in the generation of low-purity (0.01~0.1% CTCs) samples for downstream analysis.

Fluorescence-activated cell sorting (FACS) is a powerful tool for high-throughput cell analysis and can also be used to separate CTCs from peripheral blood.^{7,29} Unfortunately, commercial FACS instruments suffer from limitations associated with high operational costs, large footprints, and high shear stresses that can damage cells. Additionally, the generation of aerosols during the sorting process can lead to sample contamination.^{30–32} While FACS offers quantitative information such as size, granularity, and marker expression about individual cells, analysis occurs in a sequential manner. This means that analysis of just 1 mL of blood, containing approximately 5 billion cells, will normally take between 1 and 5 days.^{26,29} This limitation makes FACS impractical for sorting rare cells, such as CTCs, which are present in very low quantities amongst a background of abundant cells. Accordingly, CTC enrichment workflows that are both efficient and rapid are urgently needed.

Microfluidic-based fluorescence-activated cell sorters (μ FACS) have emerged as powerful tools leveraging immunofluorescence staining to efficiently separate, isolate and enrich CTCs. Unfortunately, the throughput of existing μ FACS systems strongly depends on the actuation method employed, most notably acoustophoretic,^{30,33} dielectrophoretic,^{34–36} optical,^{37,38} or hydrodynamic.³⁹ Significant efforts have therefore been directed towards enhancing sorting performance. For example, Wu and co-workers

presented an acoustofluidic device that uses tilted-angle standing surface acoustic waves to separate CTCs from blood.⁴⁰ The device achieved a recovery of over 83%, with 90% of cells being viable after sorting. While highly efficient, the low volumetric throughput (20 μ L/min) precludes widespread adoption in clinical settings. Interestingly, other technologies, such as those incorporating bubble actuators, have demonstrated the ability to sort single cells at throughputs reaching a few kHz.⁴¹ While useful, the presence of a sheath fluid leads to a 250-fold dilution, drastically lowering cell concentrations to only 4,000 cells/mL and greatly restricting practical utility in sorting CTCs from whole blood.

In general, operation at high sorting frequencies is often accompanied by reductions in sorting accuracy, which in turn increases the risk of missing “target” cells.^{30,42} To address this issue, Chiu and colleagues introduced an elegant technique called ensemble-decision aliquot ranking (eDAR).^{26,43–45} Unlike traditional sorting methods that analyse individual cells one-by-one, eDAR probes small (nL-volume) aliquots of blood containing labelled CTCs, with on-chip filtration being used to further purify isolated CTCs by removing native blood cells. That said, the current eDAR platform does not enable (off-chip) collection of CTCs for downstream analysis. This is a significant drawback. The collection of isolated cells for downstream analysis has become increasingly important since cultured CTCs have utility in various clinical applications.⁴⁶ Additionally, it should be noted that the on-chip filtration system employed within the eDAR platform may not be ideal for isolating CTC populations that exhibit an appreciable size distribution overlap with co-located blood cells.⁴⁷ Nevertheless, Chiu and co-workers have recently made additional refinements to the eDAR technique through development of a sequential eDAR platform.⁴⁸ This allows for the collection of CTCs from co-located peripheral blood mononuclear cells with good purity (>70%) and without the need for on-chip filtration. While a useful refinement, this sequential eDAR platform requires the use of density gradient centrifugation to process whole blood prior to use. Accordingly, there remains an unmet need to develop simplified workflows that enable the rapid isolation of CTCs from whole blood with excellent recovery rates and purities.

Herein, we introduce a high-throughput microfluidic rare-cell sorter (μ RCS) for the enrichment of CTCs from minimally processed whole blood. Our platform incorporates a one-dimensional (1D) complementary metal-oxide semiconductor (CMOS) image sensor capable of simultaneously detecting signals from large numbers of cells moving through 10 parallel microfluidic channels. To ensure efficient cell focusing within each channel, we employ a sheathless viscoelastic flow able to precisely align cells into single files.^{49–51} Subsequently, on-chip cell sorting is carried out using a pneumatic actuation scheme, with valve operation controlled by a field-programmable gate array (FPGA). The platform is not designed for sequential analysis and sorting of individual cells, but rather sorts cells into small aliquots, aiming to enrich rare cells of interest. To evaluate the performance of our system, we initially conduct a validation study in which fluorescent polystyrene beads (FBs) are separated and isolated from non-fluorescent beads (nFBs), with concentrations of FBs ranging from 10 to 1000 FBs/mL, and nFB concentrations ranging between 10^5 and 10^7 nFBs/mL. Subsequently, we isolate human brain glioblastoma cells (LN-229) from minimally processed whole blood, at a CTC-to-blood cell ratio of approximately 1 in 10^8 , assessing both separation efficiency and recovery rate. Significantly, the μ RCS is able to analyse 5 mL of diluted blood (equivalent to 1 mL of whole

blood) within 1 hour, producing a 73-million-fold enrichment after three rounds of sorting. Additionally, the viability of sorted cells is >96.8%, ensuring simple downstream analysis. Finally, we demonstrate the clinical utility of our device by successfully isolating CTCs from five clinical samples representing different cancer types. Tumor cells were detected in all samples, with an average abundance of only 7.6 CTCs per mL. These results highlight the effectiveness and clinical potential of our microfluidic platform for rare cell isolation, particularly for the analysis of large-volume blood samples.

RESULTS AND DISCUSSION

μ RCS Design

Figure 1 illustrates the primary components of the μ RCS, with the optical detection system being depicted in Figure 1a. Light from a 488 nm laser is shaped by a cylindrical lens to generate a light sheet that spans all primary microfluidic channels. Fluorescence emitted by cells that traverse the light sheet is collected through a 10 \times objective lens, with a 488 nm longpass filter being used to eliminate excitation photons. Fluorescence is then focused onto a 1D CMOS image sensor. The CMOS image sensor is designed to capture and analyse fluorescence signals from multiple channels simultaneously, thus enhancing analytical throughput. A custom-designed printed circuit board (PCB) is employed as both a readout circuit for the CMOS image sensor and a means of transferring data to an FPGA board through an analog-to-digital converter (ADC) board. Subsequently, acquired data are processed using a custom-developed program written in Verilog Hardware Description Language (HDL) within the FPGA. Detailed information regarding fluorescence signal acquisition and control circuit designs for FPGA-driven cell sorting are provided in Supplementary Text 1. As shown in Figure 1b, the microfluidic device comprises two layers: a control

layer and a fluidic layer. The fluidic layer is divided into two zones. Zone 1 consists of rectangular cross-section channels, and Zone 2 comprises semi-circular cross-section channels. The control layer, positioned beneath the fluidic layers, is deformed by applying pressure (2.5 bar) to block the semi-circular cross-section channels at desired positions in Zone 2. Zone 1 comprises 10 straight channels that initially run parallel to each other. These channels are 3 cm in length, 55 μ m in width, and 50 μ m in height, with an 80 μ m gap between them. Downstream of the straight channel array, the rectangular cross-section channels are separated and connected to Zone 2, where all sorting and collection operations are performed. The actuation times of solenoid valves and on-chip PDMS valves introduce a finite time delay between the detection and sorting of approximately 50 ms.⁵² The control layer (located below the fluidic layer) can then be actuated to regulate fluid flow in the fluidic layer, allowing for the movement of cells towards either the waste or collection outlets. Each sorting region contains a bifurcated channel, equipped with two valves (control valve #1 and control valve #2). Actuation of these valves enables flowing cells to be directed towards the waste outlet or the collection outlet based on a user defined detection threshold (Figure S1). When control valve #1 is closed and control valve #2 is open, cells flow towards the waste outlet. However, once a target cell is detected, control valve #1 opens and control valve #2 closes, enabling the collection of an aliquot (containing target cell) via the collection outlet. Solenoid valves, with a response time of 5 ms, are used to actuate the on-chip PDMS valves. Taking into account the PDMS membrane actuation time, a total response time of approximately 25 ms is required to switch valves #1 and #2.

μ RCS Optimization Experiments

To assess operational performance of the μ RCS, initial experiments involved the separation of 10 μ m diameter

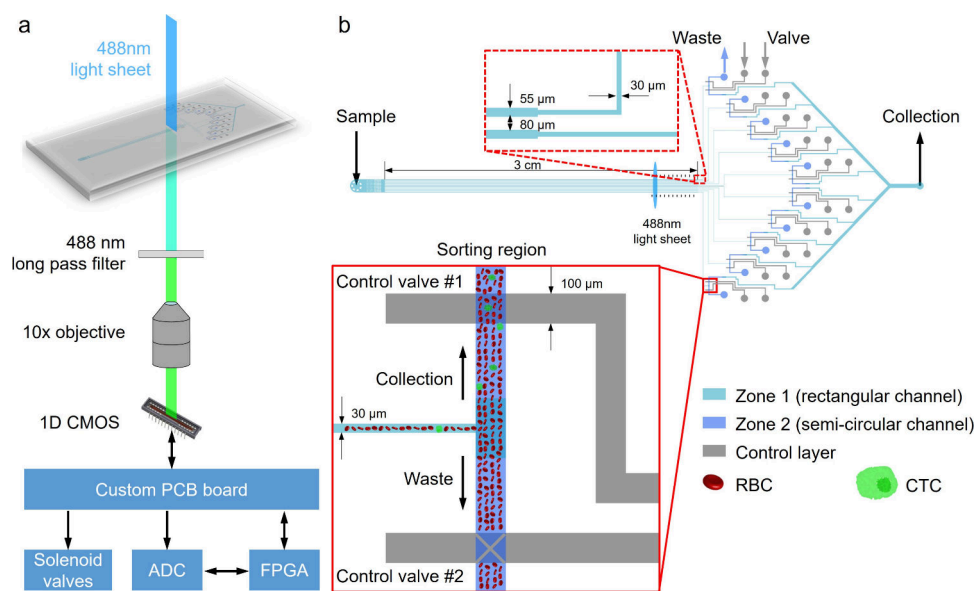


Figure 1. Schematic of the μ RCS system. (a) The system comprises several components, including a multilayer microfluidic device with 10 parallel channels, 20 solenoid valves, a 488 nm laser source, a 10 \times objective, a 488 nm longpass filter, a custom-designed readout PCB board, and an FPGA board for acquisition, real-time processing of the fluorescence signals and subsequent sorting of the target cells. (b) The microfluidic device comprises two layers: the fluidic layer and the control layer. The fluidic layer consists of two types of channels, fluid layer #1 and #2. Channels in the control layer are coloured grey. Fluid layer #1 has rectangular channels, while fluidic layer #2 contains rounded channels. The control layer regulates the flow direction of cells, enabling them to be directed either to the waste outlet or the collection outlet.

fluorescent beads and non-fluorescent beads were used as model micron-sized species that mimic typical mammalian cells. The 1D CMOS sensor provides a maximum frame rate of 4672 frames/s. While increasing the frame rate could potentially enhance the throughput of the μ RCS system, it would inevitably decrease the integration (exposure) time, consequently reducing the sensitivity. To balance detection sensitivity and throughput, the frame rate of the CMOS sensor was set to 973 frames/s, corresponding to an integration time of approximately 1 ms. The average volumetric flow rate of the sample flow was set to 500 μ L/min (equivalent to a linear velocity of approximately 300 μ m/ms), ensuring that each particle is captured in at least one image, given the pixel width of 200 μ m on the CMOS sensor and the typical particle size of 100 μ m after 10x magnification. Single-file focusing of particles was achieved through use of a viscoelastic 600 kDa polyethylene oxide (PEO) carrier fluid. Figure S2 shows the flow distribution across the microfluidic device, obtained via COMSOL simulations, confirming a uniform flow distribution across the 10 parallel channels. When the PS bead solutions were supplemented with 0.3% w/v 600 kDa PEO, particles were efficiently focused at channel centers across a wide range of particle concentrations (10^5 – 10^7 beads/mL; Figure S3a–c). In contrast, in the absence of PEO, particles could not be effectively focused under investigated conditions (Figure S3d).

Due to the Gaussian intensity distribution of the 488 nm laser beam source, the light sheet generated by the cylindrical lens is not uniform across channels. Consequently, raw signals acquired by the 1D CMOS must be corrected. Figures S4a,b show the raw and normalized signals for 10 μ m diameter FBs located within the 10 parallel channels, respectively, with Figures S4c,d displaying the corresponding fluorescence intensity distributions. The coefficient of variation (CV) of the signal decreases from 0.22 (Figure S4c) to 0.16 (Figure S4d), which is comparable

to the CV (0.18) associated with flow cytometry measurements (Figure S5). Next, we evaluated analytical throughput of the platform for detecting positive events, specifically 10 μ m FBs (Figure S6). Figure S6a to Figure S6e report the measured fluorescence intensity distributions for 10 μ m FBs at concentrations ranging from 10^5 to 3×10^6 FBs/mL. At a concentration of 2×10^6 FBs/mL, a second distribution emerges, indicating the presence of doublets (Figure S6d). Figure S6f compares the concentrations measured by the device with those obtained using conventional flow cytometry, demonstrating that the μ RCS system can reliably detect 10 μ m FBs at concentrations up to 1×10^6 FBs/mL.

Next, the sensitivity of the μ RCS system was measured using suspensions of five calibration particles containing increasing amounts of a specified fluorophore (Figure S7). The vendor-specified MESF (molecules of equivalent soluble fluorophores) intensities for five bead populations are 0, 3179, 22718, 95426, and 333766 units, respectively. Figure S7a–e displays the raw signals acquired by the CMOS sensor for each fluorescent bead population, with the resulting calibration curve being shown in Figure S7f. Based on this analysis, the limit of detection (LOD) was determined to be 18,450 MESF units at a flow rate of 500 μ L/min and a laser power of 500 mW.

Figure 2 reports performance metrics of the μ RCS system, with the purities of the initial and sorted bead solutions being determined by conventional flow cytometry. Figure 2a shows the impact of the sorting pulse duration on both enrichment factors and recovery rates, while Figure 2b reports particle purities before and after sorting (see Supplementary Text 2). As shown in Figure 2a, a sorting pulse of 15 ms is unable to sort FBs, as the valves have insufficient time to switch to an open state. As the sorting pulse duration increases, both the enrichment factor and recovery rate increase. However, for sorting pulse durations above 25 ms, the enrichment factor declines, while

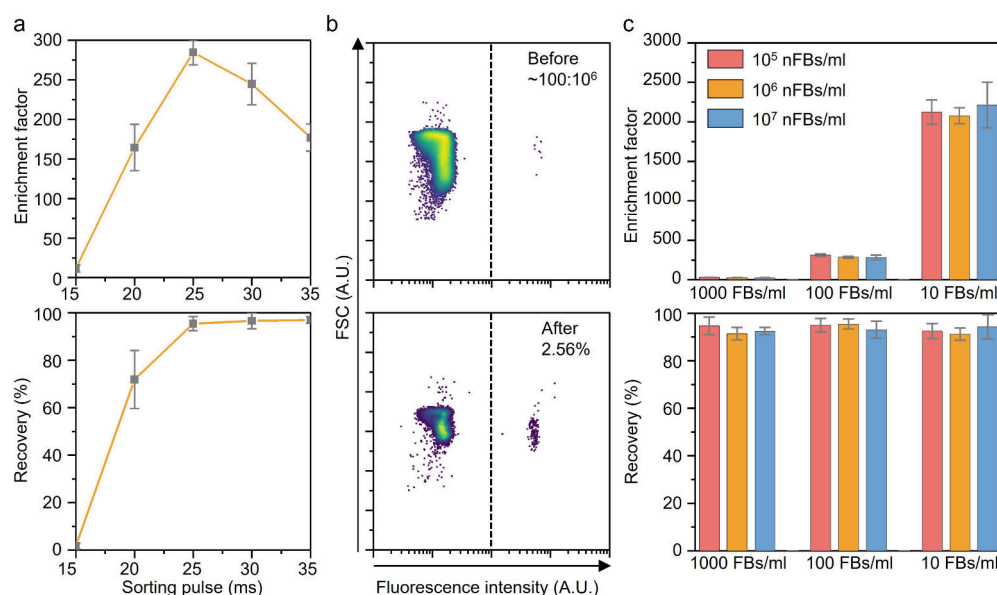


Figure 2. Performance of the μ RCS system. (a) Effect of sorting pulse duration on the enrichment factors and recoveries. Data indicate that a sorting pulse duration of 25 ms provides for optimal performance, where both the enrichment factor and recovery rate are maximized. (b) Purities of the samples before and after sorting. After sorting, purity increases from 0.01 to 2.56%. (c) Enrichment factors and recoveries under different FB concentrations (10, 100, and 1000 FBs/mL) and nFB concentrations (10^5 , 10^6 , and 10^7 nFBs/mL). Enrichment factors are independent of nFBs, suggesting that the system can efficiently enrich FBs regardless of the background particle concentration. Moreover, the recovery rates exceed 90% in all cases, indicating a high level of recovery.

the recovery rate remains constant at approximately 95%. Such a variation arises because beyond a certain sorting pulse duration, most FBs are sorted, but increasingly larger numbers of nFBs accumulate at the collection outlet. This leads to a decrease in purity within the collection outlet and consequently a decrease in the enrichment factor. The input suspension contains 100 FBs per mL and 10^6 nFBs per mL. Following sorting, the purity increases over two orders of magnitude from 0.01% to 2.56% (Figure 2b). Figure 2c additionally presents enrichment factors and recoveries for concentrations of between 10 and 1000 FBs/mL and 10^5 and 10^7 nFBs/mL. Enrichment factors were found, to be dependent on FB concentration but independent of (background) nFB concentration. Specifically, average enrichment factors for concentrations of 1000, 100, and 10 FBs/mL were determined to be 26, 293, and 2138, respectively. Additionally, recovery rates consistently exceeded 90% for all tested conditions. Finally, since the error bars in Figure 2c represent the standard deviation of three independent measurements for each bead concentration, recoveries remain above 90%, with only minor variation between runs.

Rare Cell Enrichment

After characterizing the μ RCS system using beads, we next assessed performance when enriching rare cells. Briefly, patient-derived human brain glioblastoma cells (LN229) were used as model CTCs and labelled with fluorescent antibodies. To minimize autofluorescence plasma was removed prior to analysis, with the remaining cell suspension being diluted with 1 \times phosphate-buffered saline (PBS) and supplemented

with 0.3% w/v PEO. Next, fluorescently labelled LN229 cells were added to a concentration of 10 cells/mL, resulting in a CTC-to-blood cell ratio of approximately 1 to 10^8 . Sample was then injected into the μ RCS system and subjected to three rounds of sorting. Following each round, the collected sample was diluted to a total volume of 5 mL using 1 \times PBS, supplemented with 0.3% w/v PEO. After experimentation, the eluent (collected sample) was analysed using conventional flow cytometry. To assess the effectiveness of the sorting process and quantify LN229 enrichment, sorted samples were compared with the unprocessed input sample (Figure 3). CTCs within the cell mixture are identified using a two-parameter density plot of forward scatter (FSC-A) signal vs fluorescence at 525 nm (FITC-A). The gating strategy used to distinguish CTCs from blood cells is described in Supplementary Text 3 and Figure S8. More specifically, flow cytometry was used to gate events based on the fluorescence signal at 525 nm (FITC-A), derived from the conjugated fluorescently-labelled EpCAM antibodies, and size difference between CTCs and blood cells. The false positive rate was defined as the fraction of events from EpCAM-negative control samples that fall within the CTC gate. Analysis of minimally processed blood from healthy donors showed no events in this gate (Figure S8), indicating a false positive rate below the detection limit of the system.

Analysis of eluent collected after each sorting round confirmed the efficient separation of CTCs from blood (Figure 3b–d). Specifically, after the third sorting round, the purity of the collected sample had increased from 10^{-6} % (initial sample) to 73.40% (Figure 3d). This corresponds to an enrichment

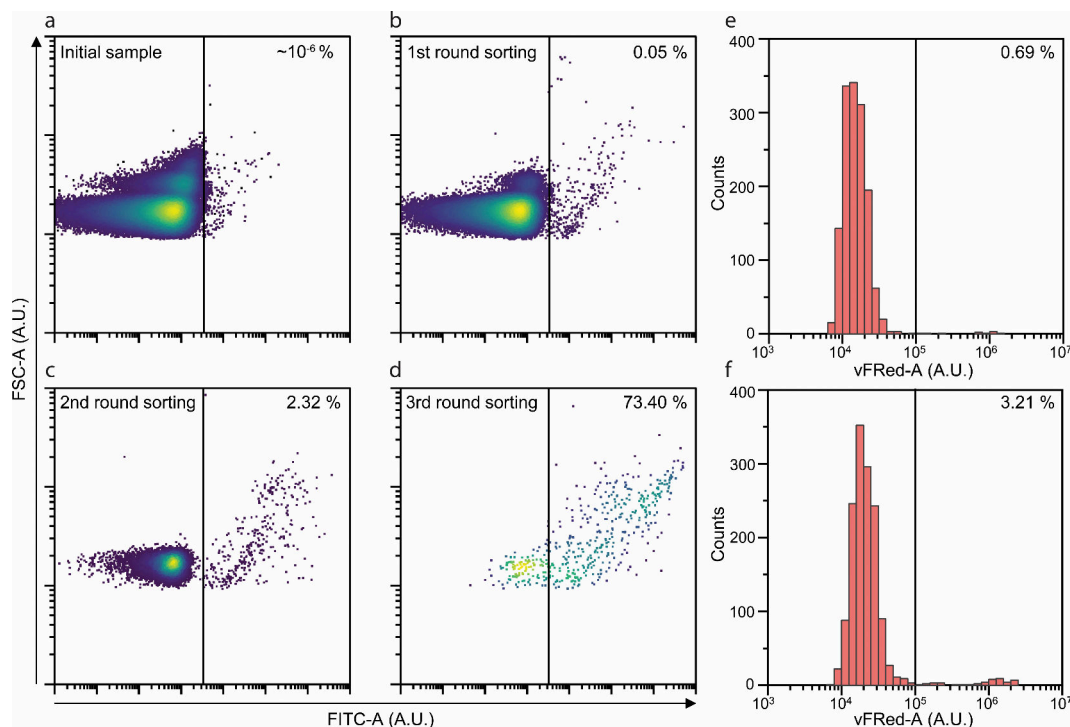


Figure 3. Flow cytometry scatter plots reporting the enrichment of CTCs after multiple sorting rounds. CTCs, spiked into diluted blood at a ratio of $1:10^8$ (CTCs to blood cells), experienced significant enrichment after three sorting rounds. Scatter plots of FSC-A vs FITC-A show the percentages of the RBCs and CTCs before sorting (a) and after the first (b), the second (c) and third (d) sorting rounds. These data demonstrate the progressive enrichment of CTCs with each sorting round. After three sorting rounds, a notable improvement in CTC purity is achieved, with a purity value of 73.40%. Fluorescence intensity histograms of LN229 cells in the control sample (e) and the sample collected after sorting (f). Both samples showed similar viability values (99.31 and 96.79%), highlighting the fact that the microfluidic sorting system does not impart significant stress on the cells.

of almost eight orders of magnitude. Such a high level of enrichment confirms the high efficiency of the μ RCS in isolating and enriching CTCs from blood. Notably, the entire process, encompassing blood pre-processing, is completed within just 1 hour. In contrast, conventional flow cytometry analysis would typically take 5 days to do the same job, assuming a throughput of 12,000 cells per second.^{26,29} To complete this evaluation, we assessed the viability of collected cells post sorting. This is important since mechanical stresses arising from shear/fluid forces can lead to gene upregulation and even trigger apoptotic responses.^{53,54} To evaluate CTC viability, we processed a sample containing fluorescently labelled LN229 cells at a concentration of 1000 cells/mL to ensure statistical significance. Both the control sample (comprising cells incubated at room temperature) and the sample collected after a single round of sorting were subjected to staining using a Zombie NIR™ viability assay. Samples were then analysed by flow cytometry, detecting fluorescence at 690 nm. Such an analysis revealed that processing through the μ RCS leads to negligible cellular damage, with viability after sorting being 96.79%, a value comparable to the viability of the control sample (99.31%, Figure 3e,f).

Finally, we used the μ RCS system applied to enrich and purify circulating tumor cells harvested from the blood of cancer patients. 1 mL blood samples were collected from five patients diagnosed with small cell lung cancer, non-small cell lung cancer, or breast cancer. Each sample was stained with an EpCAM Alexa 488-labelled antibody and processed through the device at a flow rate of 500 μ L/min. Enriched cells collected from device outlets were subsequently analysed by flow cytometry

(Figure 4a). CTCs were detected in all five samples, with 8, 12, 4, 6 and 8 cells being detected in Samples 1, 2, 3, 4 and 5, respectively (Figure 4b). The number of CTCs detected using the μ RCS system was validated against measurements obtained using the FDA approved *CellSearch* system (Figure 4b). For the μ RCS system, 1.0 mL of whole blood was processed per sample, whereas 7.5 mL of whole blood was analysed using the *CellSearch* system, as per the manufacturer's instructions. To allow for a direct comparison, all counts in Figure 4b are reported as CTCs per mL of whole blood. The mean CTC count (per mL) for all samples taken together was 7.6 for the μ RCS system and 3.1 for *CellSearch*, demonstrating that the μ RCS system is capable of isolating and detecting CTCs from clinical samples, with equivalent (or even higher) sensitivity than the *CellSearch* system. Nevertheless, larger clinical studies will be required to validate both sensitivity and robustness more comprehensively.

CONCLUSIONS

To conclude, the developed high-throughput fluorescence-activated sorting platform offers a novel approach for isolating rare cells, specifically CTCs, from minimally processed whole blood. The platform integrates CTC detection, analysis and separation with a single compact system, offering an "all-in-one" solution for CTC analysis. The platform comprises a fluorescence-based optical system, a microfluidic processor consisting of 10 parallel channels, a 1D CMOS image sensor with a custom-designed readout circuit that can drive twenty solenoid valves, and a dedicated logic circuit (FPGA board)

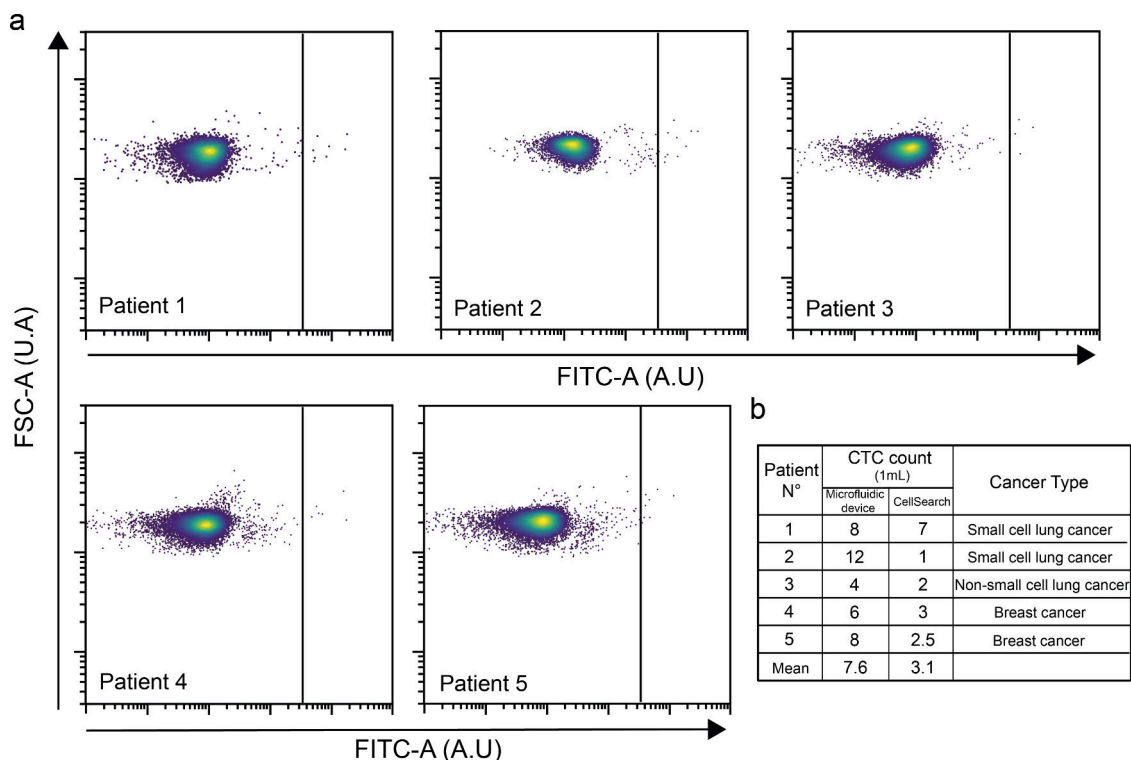


Figure 4. Detection and enumeration of CTCs in patient blood samples using the μ RCS system and the *CellSearch* instrument. (a) Representative flow cytometry plots (FSC-A vs. FITC-A) for CTC detection in blood samples from five cancer patients, following enrichment with the microfluidic device and staining with Alexa 488-labelled anti-EpCAM antibody. (b) Table summarizing CTC counts per milliliter of blood detected in each patient sample by both the μ RCS system and *CellSearch*, along with a statement of the corresponding cancer type. The μ RCS system consistently detected CTCs in all samples, with counts on the same order of magnitude as those obtained by the *CellSearch* platform.

for real-time data acquisition, signal processing and sorting of the target species. Significantly, the system operates at a volumetric throughput of 500 $\mu\text{L}/\text{min}$, allowing the complete analysis of 5 mL of a (5-fold diluted) blood sample in less than 30 minutes, achieving an enrichment factor in excess of 72 million while maintaining a purity of 73.40%. Importantly, the platform maintains high cell viability post analysis, with sorted CTCs exhibiting a viability of 96.79%, rendering them suitable for downstream molecular analysis and functional studies. Significantly, the μRCS does not suffer from channel fouling/blocking issues when processing large sample volumes or highly concentrated fluids under the operating conditions studied. The μRCS avoids such issues by combining a valve-based sorting mechanism with modular parallel units that distribute the sample load and dynamically bypass congested regions. Such an approach prevents backpressure build-up and allows continuous processing without channel blockage or excessive mechanical stress on cells, ensuring high viabilities and capture efficiencies. Sorting in the μRCS platform involves the generation of small fluid aliquots that may contain zero, one, or multiple target cells. Target (CTCs) and non-target (blood cells) cells will simultaneously occupy a given aliquot, and thus the aliquot volume will determine purity. Accordingly, the ability to generate small volume aliquots provides a direct route to improving purity. In the current study, after three sorting rounds the platform achieves a purity of $\sim 73\%$ and a recovery $>90\%$ while maintaining cell viability at $\sim 97\%$. These values are entirely compatible with many downstream assays such as short-term culture, drug testing on enriched populations, or bulk DNA/RNA sequencing. When compared to other physical separation technologies that depend on size, deformability or inertial flow effects, μRCS provides for superior performance metrics, including outstanding enrichment factors (8 orders of magnitude), and excellent purities ($\sim 73.4\%$) and recovery rates ($>90\%$).¹¹

Compared to conventional flow cytometry, the μRCS system offers multiple advantages. First, it operates at high throughput due to its modular integration of ten sorting units. This eliminates the need for sequential analysis of individual cells in a single-file format. Second, the μRCS system can be directly interfaced with downstream analysis, enabling various applications, including in vitro CTC culture, drug sensitivity testing and gene sequencing. Third, the adoption of valve-based sorting ensures that cells are not subjected to excess stress. Fourth, the μRCS is intended to function as a high-throughput upstream enrichment module that processes minimally processed whole-blood samples prior to detailed analytical characterization. In this context, it complements conventional FACS platforms, which are almost always applied to enriched cell suspensions rather than to large volumes of blood containing a complex background of erythrocytes and leukocytes.

Looking forward, it is important to note that the μRCS architecture is modular and can be expanded by simply increasing the number of channel-valve units. Practical limits, however, exist. First, the hydraulic network must preserve a uniform flow distribution and stable pressure across all channels. As channel numbers increase, small variations in hydrodynamic resistance can lead to measurable differences in volumetric flow rates and sorting performance. Second, the optical field of view, determined by the objective magnification and CMOS line sensor dimensions, constrains the maximum number of channels that can be imaged

with adequate spatial separation, while still operating at the high frame rates required for real-time sorting. As an approximate design guideline, a low-magnification objective (4 \times) together with the CMOS line sensor (28.672×0.200 mm) yields a field of view of 7.2 mm \times 50 μm . This is sufficient to image twenty $50\mu\text{m}$ -wide microchannels with an inter-channel spacing of 15 μm . Under the present operating conditions, the 10-channel RCS processes 0.5 mL/min of whole blood (5-fold diluted sample at 2.5 mL/min), i.e., about 30 mL per hour. Extending the device to 20 parallel channels would increase the analytical throughput to ~ 1.0 mL/min, corresponding to approximately 60 mL of whole blood per hour. This analysis illustrates that moderate increases in channel number beyond the current 10-channel configuration are technically feasible using the same optical concept.

Benchmarking the μRCS system against the FDA-approved *CellSearch* platform confirms its clinical utility, with the analyses of blood from a cohort of five cancer patients demonstrating that the system can detect equivalent (or higher) numbers of CTCs. That said, it should be noted that the current dataset is too small to support definitive conclusions, and larger-scale clinical studies will be required to properly quantify diagnostic performance. Since the μRCS system provides for both high purity and enrichment, downstream applications such as cell culture, drug sensitivity assays, and sequencing can be directly performed without additional purification steps. In contrast, the *CellSearch* platform typically generates a substantial leukocyte background, making downstream molecular analyses far more challenging.

The biological validation presented here relies on EpCAM-based detection, which may not capture the full phenotypic heterogeneity of CTCs. Accordingly, we anticipate that future implementations of our microfluidic cell sorter will incorporate additional epithelial and mesenchymal markers. More specifically, we envisage replacing or complementing EpCAM with alternative antibody panels, for example targeting EGFR, HER2 or vimentin, to enable efficient enrichment of EpCAM-low or EpCAM-negative CTC subpopulations, while using an identical fluorescence-based sorting principle.

Finally, a key feature of the μRCS system is its ability to seamlessly integrate sample preparation, high-CTC identification, and sorting within a single platform. Indeed, we are currently advancing single-cell recovery from the microfluidic device to enable downstream applications such as PCR and next-generation sequencing. After three rounds of sorting, the enriched fraction exhibits a purity of approximately 73%, with a recovery greater than 90% and post-sorting viability close to 97%. These values are compatible with a range of downstream uses, including bulk molecular assays and functional studies on enriched CTC populations, for which high viability is more important than the complete removal of all background cells. For applications that require near-single-cell purity, such as certain single-cell genomic protocols,⁵⁵ the enriched output can be coupled to an additional purification step (for example, single-cell isolation or droplet-based partitioning), which is facilitated by the high starting enrichment provided by the μRCS platform. These efforts aim to deepen our understanding of CTC heterogeneity and the molecular underpinnings of metastasis, potentially identifying clinically relevant CTC subtypes linked to prognosis and therapeutic response. Overall, the developed high throughput μRCS system represents a highly promising technology for efficiently enriching and analyzing CTCs from whole blood.

MATERIALS AND METHODS

Device Design and Fabrication

The microfluidic device was designed using AutoCAD 2018 (Autodesk, San Rafael, USA) and printed onto film photomasks (Micro Lithography Services, Chelmsford, UK). Flow fields were designed and optimized using COMSOL Multiphysics 5.5 (COMSOL, Burlington, USA). The multilayer sorting device comprises a control and a fluidic layer consisting of two different channels (Zone 1 and Zone 2) (Figure 1b).

First, the 15 μm deep control layer master mold was fabricated using standard photolithographic techniques. SU-8 2010 photoresist (MicroChem, Westborough, USA) was spin-coated onto a 4-inch diameter silicon wafer (Siegert Wafer, Aachen, Germany). A spin speed of 2000 rpm resulted in the formation of a 15 μm thick resist layer. The spin-coated wafer was then baked on a hot plate at 65 $^{\circ}\text{C}$ for one minute and 95 $^{\circ}\text{C}$ for four minutes. Channel patterns in the mask were transferred to the SU-8 coated wafer by UV exposure for 30 seconds. Subsequently, the wafer was baked at 95 $^{\circ}\text{C}$ for four minutes to facilitate cross-linking of the exposed SU-8 photoresist. Patterned structures were developed using 1-methoxy-2-propyl acetate (Sigma-Aldrich, Buchs, Switzerland) to remove regions of unexposed photoresist. Finally, the wafer was thoroughly rinsed with isopropyl alcohol and water, followed by drying with pressured air. The fabricated mold was then hard-baked at 150 $^{\circ}\text{C}$ for 10 minutes.

To fabricate the master mold for Zone 2 of the fluidic layer, AZ40XT photoresist (Micro Resist Technology, Berlin, Germany) was spin-coated on a 4-inch diameter silicon wafer (Siegert Wafer, Aachen, Germany) to form a 30 μm thick layer. The spin-coated wafer was then baked at 126 $^{\circ}\text{C}$ on a hot plate for seven minutes. Channel patterns in the photomask were transferred to the wafer by UV exposure for 30 seconds. After exposure, the wafer was left inside a closed vessel containing wet paper towels for 8 hours. This rehydration step was essential to prevent cracks and bubbles forming within the resist layer. The rehydrated wafer was post-baked at 105 $^{\circ}\text{C}$ for 100 seconds to facilitate cross-linking of the exposed AZ40XT photoresist. The patterned structures were developed using AZ300 MIF developer (Micro Resist Technology, Berlin, Germany) to remove exposed photoresist. The wafer was thoroughly rinsed with water, followed by drying with pressured air. A semi-circular channel cross section was necessary to operate the valves with minimum leakage. Accordingly, the developed wafer was heated at 142 $^{\circ}\text{C}$ overnight to allow the reflow of the developed structures.

The master mold for Zone 1 was fabricated using standard photolithographic techniques on top of the Zone 2 patterned mold. First, SU-8 50 photoresist (Micro Resist Technology, Berlin, Germany) was spin-coated onto the silicon wafer containing structures for Zone 2. A spin speed of 2000 rpm resulted in a 50 μm thick resist layer. The spin-coated wafer was baked at 65 $^{\circ}\text{C}$ for one minute and 95 $^{\circ}\text{C}$ for four minutes. Channel patterns in the photomask were aligned to patterns in Zone 2 using a mask aligner (SUSS, Munich, Germany). Next, the channel patterns in the mask were transferred to the wafer using UV radiation for 30 seconds. The patterned structures were developed using 1-methoxy-2-propyl acetate (Sigma-Aldrich, Buchs, Switzerland) to remove unexposed resist. Finally, the wafer was rinsed with isopropyl alcohol and water, followed by drying using pressured air. Finally, both control and fluidic layer molds were placed into a desiccator containing a beaker of chlorotrimethylsilane (Sigma-Aldrich, Buchs, Switzerland) solution and incubated for at least 5 hours at a pressure of 150 mbar. The process of mold functionalization with chlorotrimethylsilane aids peeling of cured PDMS from the mold.

Microfluidic devices were made using standard soft lithographic methods.⁵⁶ PDMS mixtures were prepared at 20:1 and 5:1 (wt/wt) PDMS base to curing agent (Sylgard 184, Dow Corning, Midland, USA) ratios when fabricating the control and fluidic layer, respectively. Both mixtures were first degassed in a desiccator for 30 minutes. Next, the 5:1 mixture was poured onto the fluidic layer mold and the 20:1 mixture was spin-coated at 2600 rpm on the control layer mold for 40 seconds. Both

wafers were then baked at 70 $^{\circ}\text{C}$ for 25 minutes. Next, the PDMS fluidic layer was peeled off the wafer and diced. Diced PDMS structures were carefully aligned with the control layer under a stereoscope. The aligned devices were then cured at 70 $^{\circ}\text{C}$ overnight, allowing the layers to bond through the diffusion of the curing agent from the fluidic to the control layer. Finally, cured devices were peeled from the control layer mold. A Gauge 22 puncher (I and Peter Gonano, Niederösterreich, Austria) was used to create inlet and outlet ports in the structured PDMS substrate. Finally, the structured PDMS substrate and a 24 \times 75 \times 1 mm glass slide (Menzel-Glaser, Braunschweig, Germany) were treated in a Zepto air plasma chamber (Diener Electronic, Ebhausen, Germany) for 1 minute and contacted. The entire assembly was then placed on a hot plate at 120 $^{\circ}\text{C}$ for 2 hours to strengthen bonding of the PDMS substrate to the glass slide.

Device Operation and Data Acquisition

Blood samples were loaded into a 10 mL Hamilton syringe (Hamilton Laboratory Products, Reno, USA), and delivered into the microfluidic device using neMESYS precision syringe pumps (CETONI, Korbussen, Germany) at a volumetric flow rate of 500 $\mu\text{L}/\text{min}$. Suspensions of 10 μm FBs (FC06F, Fishers, Indiana, USA) and nFBs (Sigma-Aldrich, Steinheim, Germany), were prepared at concentrations ranging from 10 to 1000 FBs/mL and 10^5 to 10^7 nFBs/mL, respectively. A Quantum Alexa Fluor 488 MESF calibration kit (Bangs Laboratories, Fishers, USA) consisting of five microsphere populations labelled with increasing amounts of a specified fluorochrome, was used for intensity calibration measurements.

The microfluidic device was mounted on an Eclipse Ti-E inverted microscope (Nikon, Zurich, Switzerland), integrating a x - y motorized stage (Mad City Labs, Maddison, USA) to facilitate observation and positioning with the laser excitation sheet. A 488 nm laser beam (Coherent Genesis MX, Glasgow, UK) was transmitted through an acoustooptical tuneable filter (AOTF nC-400-650-TN, AA Opto-electronic, Orsay, France) connected to an RF driver (AA Opto-electronic, Orsay, France). The laser beam was focused to a light sheet with a width approximately equal to the average cell diameter (~ 15 μm) using a cylindrical lens (LJ1558RM-A, Thorlabs, Lubeck, Germany). Fluorescence photons were collected via a 10 \times , 0.3 NA Plan Fluor objective (Nikon, Zurich, Switzerland), passed through a 488 nm longpass filter (AHF, Tubingen, Germany) to reject the excitation light and focused by the microscope tube lens onto an S11639 CMOS sensor (Hamamatsu, Solothurn, Switzerland). A custom-designed PCB was used both as a readout circuit for the CMOS image sensor and for transferring the acquired data to an FPGA board via an ADC board. Data were processed in the FPGA using a custom-developed program written in Verilog HDL (Vivado Design Suite 2020, Xilinx, San Jose, USA). And 20 Solenoid valves (MH1, Festo, Lupfig, Switzerland) were controlled parallelly by the FPGA.

Viscoelastic Fluid Preparation and Characterization

Viscoelastic stock solutions were prepared by fully dissolving 600 kDa polyethylene oxide (PEO, Sigma-Aldrich, Buchs, Switzerland) in 1 \times PBS buffer (Thermo Fisher Scientific, Reinach, Switzerland) to a concentration of 1% (w/v). Stock solutions were aged at room temperature for 1 week to ensure uniform viscosity. Before each experiment, a 0.3% w/v PEO concentration solution was prepared by diluting the 1% stock PEO solution into the particle/cell suspensions. This step was essential to facilitate focusing of cells/particles in a sheathless manner. Viscosities (Figure S8) were measured at room temperature using an MCR 502 compact rheometer equipped with a double gap (DG 26.7) tool (Anton Paar, Ostfildern, Germany).

Flow Cytometry Measurements

Flow cytometry measurements were conducted using a CytoFLEX flow cytometer (Beckman Coulter, Pasadena, USA). Forward scattered (FSC-A) signal vs fluorescence at 525 nm (FITC-A) was used for gating. A 423106 Zombie NIR fixable viability kit (BioLegend,

San Diego, California, USA) was used for live/dead cell testing. Cell viability analysis was conducted using fluorescence emitted at 690 nm (vFRed-A). For all measurements, the sample flow rate was set to 30 $\mu\text{L}/\text{min}$. Data were acquired using CytExpert software (Beckman Coulter, Pasadena, USA) and subsequently processed using FlowJo software (FlowJo, Ashland, USA).

Preparation of Fluorescently Labelled LN229 Cells

A human origin glioblastoma cell line LN229 was cultured in DMEM medium (Invitrogen Life Technologies, Basel, Switzerland) supplemented with 10% FBS at 37 °C in a humidified atmosphere with 5% CO_2 . Cells were harvested by brief exposure to 0.25% trypsin/1-mM ethylenediaminetetraacetic acid (EDTA) (Thermo Fisher Scientific, Reinach, Switzerland). Cells were washed with 0.1% bovine serum albumin (BSA)/phosphate-buffered saline (PBS) and treated with 1 $\mu\text{g}/\text{mL}$ of Alexa Fluor 488 anti-human EGFR Ab (Biolegend, San Diego, USA) for 30 minutes at 4 °C, then washed with PBS. Fluorescently labelled cells were analysed using the CytoFlex flow cytometer (Beckman Coulter, Pasadena, USA).

Blood Sample Collection

Blood samples were collected in EDTA tubes and obtained from the blood donation centre, Blutspende Zürich (Schlieren, Switzerland). The study was conducted in accordance with the principles of the Declaration of Helsinki and the project was approved by the Swiss Association of Research Ethics Committees (BASEC-Nr: 2019-01721).

Preparation of Blood Samples

1 mL of blood was centrifuged at 400 g for 5 minutes at 4 °C to separate plasma from cells. The plasma was discarded, leaving behind the remaining cells. Next, 1 \times PBS was added to the cell solution to a final volume of 5 mL. The suspension was centrifuged again at 400 g for 5 minutes at 4 °C to remove any residual plasma components. Finally, the supernatant was aspirated, and RBCs were diluted with 1 \times PBS to a total volume of 5 mL. During this step, 0.3% w/v PEO was supplemented to the solution to aid in focusing of cells.

CellSearch System

CTC enumeration was performed using the CellSearch system (Menarini Silicon Biosystems, Huntingdon Valley, PA, USA) on samples obtained from five patients and two healthy donors. For each sample, the standard CellSearch protocol was applied. Specifically, 7.5 mL of undiluted whole blood was collected in CellSave preservative tubes (Menarini Silicon Biosystems) to preserve cell integrity for up to 96 hours. Samples were stored at room temperature prior to processing. Following storage, 6.5 mL of CellSearch Circulating Tumor Cell Kit Dilution Buffer (Menarini Silicon Biosystems) was added to each sample. The mixtures were then centrifuged at 800 g for 10 minutes. Subsequently, samples were processed using the CellTracks AutoPrep System in conjunction with the CellSearch Circulating Tumor Cell Kit (Menarini Silicon Biosystems). The kit utilizes ferrofluid nanoparticles coated with anti-EpCAM antibodies to capture epithelial cells, as well as fluorescently labelled antibodies for cell identification: phycoerythrin-conjugated cytokeratin (CK) antibodies, and allophycocyanin-conjugated CD45 antibodies to distinguish CTCs from leukocytes. Cells were classified as CTCs if they were EpCAM⁺/CK⁺/CD45⁻ with nuclear morphology consistent with intact cells.

■ ASSOCIATED CONTENT

Supporting Information

The Supporting Information is available free of charge at <https://pubs.acs.org/doi/10.1021/acssensors.5c04510>.

Supporting Information accompanies this article and provides additional experimental and technical details.

It describes the design and operation of the electronics and control logic for the sorter, including the CMOS line sensor, signal amplification and digitization, and FPGA-based timing and valve actuation. It also defines purity, enrichment factor, and recovery, and further explains the gating strategy used to identify CTCs in flow cytometry. It also includes figures illustrating the valve-sorting sequence, COMSOL simulations of flow in the parallel channels, bead focusing with and without PEO, and fluorescence signal normalization and comparison to a commercial flow cytometer. Additional figures present throughput and sensitivity measurements with fluorescent beads, viscosity measurements of the PEO solution, and full circuit diagrams for the sensor readout, amplifier, and sorter electronics (PDF)

■ AUTHOR INFORMATION

Corresponding Authors

Stavros Stavrakis – Department of Chemistry and Applied Biosciences, Institute for Chemical and Bioengineering, Zürich 8093, Switzerland; orcid.org/0000-0002-0888-5953; Email: stavros.stavrakis@chem.ethz.ch

Andrew J. deMello – Department of Chemistry and Applied Biosciences, Institute for Chemical and Bioengineering, Zürich 8093, Switzerland; orcid.org/0000-0003-1943-1356; Email: andrew.demello@chem.ethz.ch

Authors

Yingchao Meng – Department of Chemistry and Applied Biosciences, Institute for Chemical and Bioengineering, Zürich 8093, Switzerland; orcid.org/0000-0001-9097-0868

Mahmut Kamil Aslan – Department of Chemistry and Applied Biosciences, Institute for Chemical and Bioengineering, Zürich 8093, Switzerland; orcid.org/0000-0003-3779-6797

Qingmei Xu – Department of Chemistry and Applied Biosciences, Institute for Chemical and Bioengineering, Zürich 8093, Switzerland; School of Integrated Circuits, Peking University, Beijing 100871, China

Sarah Duclos Ivetch – Department of Chemistry and Applied Biosciences, Institute for Chemical and Bioengineering, Zürich 8093, Switzerland

Yanan Zhang – Department of Neurology, University Hospital Zürich, Zürich 8091, Switzerland; Clinical Neuroscience Center, University of Zürich, Zürich 8091, Switzerland

Alexander Ring – Clinic for Medical Oncology and Hematology, University Hospital Zurich, Zürich 8091, Switzerland

Tobias Weiss – Department of Neurology, University Hospital Zürich, Zürich 8091, Switzerland; Clinical Neuroscience Center, University of Zürich, Zürich 8091, Switzerland

Complete contact information is available at:

<https://pubs.acs.org/doi/10.1021/acssensors.5c04510>

Author Contributions

[#]Y.M. and M.K.A. contributed equally to this paper. Y.M. and S.S. conceived the idea for the project. S.S. and A.d.M. supervised the overall project. Y.M. performed all microfluidic experiments. M.K.A. was responsible for manufacturing the sorting electronics and conducting preliminary experiments, as well as developing the real-time analysis software. Q.X.

performed the microfluidic experiments related to CTCs in patients' blood. S.D.I. performed experiments using the *CellSearch* platform. Y.Z. cultured the glioblastoma cell lines. T.W. provided the glioblastoma cell lines, and A.R. provided the blood samples from cancer patients at the University Hospital Zurich. The manuscript was written by Y.M., S.S., and A.d.M.

Notes

The authors declare that they have no known competing financial interests or personal relationships that could have appeared to influence the work reported in this paper.

ACKNOWLEDGMENTS

The authors would like to acknowledge financial support from ETH Zürich.

REFERENCES

- (1) Chaffer, C. L.; Weinberg, R. A. A Perspective on Cancer Cell Metastasis. *Science* **2011**, *331* (6024), 1559–1564.
- (2) Allard, W. J.; Matera, J.; Miller, M. C.; Repollet, M.; Connelly, M. C.; Rao, C.; Tibbe, A. G.; Uhr, J. W.; Terstappen, L. W. Tumor Cells Circulate in the Peripheral Blood of All Major Carcinomas but Not in Healthy Subjects or Patients With Nonmalignant Diseases. *Clin. Cancer Res.* **2004**, *10* (20), 6897–6904.
- (3) Botteri, E.; Sandri, M. T.; Bagnardi, V.; Munzone, E.; Zorzino, L.; Rotmensz, N.; Casadio, C.; Cassatella, M. C.; Esposito, A.; Curigliano, G.; Salvatici, M.; Verri, E.; Adamoli, L.; Goldhirsch, A.; Nolè, F. Modeling the Relationship between Circulating Tumour Cells Number and Prognosis of Metastatic Breast Cancer. *Breast Cancer Res. Treat.* **2010**, *122* (1), 211–217.
- (4) Micalizzi, D. S.; Maheswaran, S.; Haber, D. A. A Conduit to Metastasis: Circulating Tumor Cell Biology. *Genes Dev.* **2017**, *31* (18), 1827–1840.
- (5) Fabisiewicz, A.; Grzybowska, E. CTC Clusters in Cancer Progression and Metastasis. *Med. Oncol.* **2016**, *34* (1), 12.
- (6) Hou, H. W.; Warkiani, M. E.; Khoo, B. L.; Li, Z. R.; Soo, R. A.; Tan, D. S. W.; Lim, W. T.; Han, J.; Bhagat, A. A. S.; Lim, C. T. Isolation and Retrieval of Circulating Tumor Cells Using Centrifugal Forces. *Sci. Rep.* **2013**, *3* (1), No. 1259.
- (7) Bhagwat, N.; Dulmage, K.; Pletcher, C. H.; Wang, L.; DeMuth, W.; Sen, M.; Balli, D.; Yee, S. S.; Sa, S.; Tong, F.; Yu, L.; Moore, J. S.; Stanger, B. Z.; Dixon, E. P.; Carpenter, E. L. An Integrated Flow Cytometry-Based Platform for Isolation and Molecular Characterization of Circulating Tumor Single Cells and Clusters. *Sci. Rep.* **2018**, *8* (1), 5035.
- (8) Chen, Y.; Li, P.; Huang, P. H.; Xie, Y.; Mai, J., D.; Wang, L.; Nguyen, N. T.; Huang, T. J. Rare Cell Isolation and Analysis in Microfluidics. *Lab. Chip* **2014**, *14* (4), 626–645.
- (9) Nam, J.; Tan, J. K. S.; Khoo, B. L.; Namgung, B.; Leo, H. L.; Lim, C. T.; Kim, S. Hybrid Capillary-Inserted Microfluidic Device for Sheathless Particle Focusing and Separation in Viscoelastic Flow. *Biomicrofluidics* **2015**, *9* (6), No. 064117.
- (10) Dong, Y.; Skelley, A. M.; Merdek, K. D.; Sprott, K. M.; Jiang, C.; Pierce, W. E.; Lin, J.; Stocum, M.; Carney, W. P.; Smirnov, D. A. Microfluidics and Circulating Tumor Cells. *J. Mol. Diagn.* **2013**, *15* (2), 149–157.
- (11) Descamps, L.; Le Roy, D.; Deman, A. L. Microfluidic-Based Technologies for CTC Isolation: A Review of 10 Years of Intense Efforts towards Liquid Biopsy. *Int. J. Mol. Sci.* **2022**, *23* (4), 1981.
- (12) Kolostova, K.; Pinkas, M.; Jakabova, A.; Pospisilova, E.; Svobodova, P.; Spicka, J.; Cegan, M.; Matkowski, R.; Bobek, V. Molecular Characterization of Circulating Tumor Cells in Ovarian Cancer. *Am. J. Cancer Res.* **2016**, *6* (5), 973–980.
- (13) Lin, D.; Shen, L.; Luo, M.; Zhang, K.; Li, J.; Yang, Q.; Zhu, F.; Zhou, D.; Zheng, S.; Chen, Y.; Zhou, J. Circulating Tumor Cells: Biology and Clinical Significance. *Signal Transduction Targeted Ther.* **2021**, *6* (1), 1–24.
- (14) Qiao, Z.; Teng, X.; Liu, A.; Yang, W. Novel Isolating Approaches to Circulating Tumor Cell Enrichment Based on Microfluidics: A Review. *Micromachines* **2024**, *15* (6), 706.
- (15) Cho, H.; Kim, J.; Song, H.; Sohn, K. Y.; Jeon, M.; Han, K. H. Microfluidic Technologies for Circulating Tumor Cell Isolation. *Analyst* **2018**, *143* (13), 2936–2970.
- (16) Harouaka, R. A.; Nisic, M.; Zheng, S. Y. Circulating Tumor Cell Enrichment Based on Physical Properties. *SLAS Technol.* **2013**, *18* (6), 455–468.
- (17) Jack, R. M.; Grafton, M. M.; Rodrigues, D.; Giraldez, M. D.; Griffith, C.; Cieslak, R.; Zeinali, M.; Kumar Sinha, C.; Azizi, E.; Wicha, M.; Tewari, M.; Simeone, D. M.; Nagrath, S. Ultra-Specific Isolation of Circulating Tumor Cells Enables Rare-Cell RNA Profiling. *Adv. Sci.* **2016**, *3* (9), No. 1600063.
- (18) Kalyan, S.; Torabi, C.; Khoo, H.; Sung, H. W.; Choi, S. E.; Wang, W.; Treutler, B.; Kim, D.; Hur, S. C. Inertial Microfluidics Enabling Clinical Research. *Micromachines* **2021**, *12* (3), 257.
- (19) Warkiani, M. E.; Khoo, B. L.; Wu, L.; Tay, A. K. P.; Bhagat, A. A. S.; Han, J.; Lim, C. T. Ultra-Fast, Label-Free Isolation of Circulating Tumor Cells from Blood Using Spiral Microfluidics. *Nat. Protoc.* **2016**, *11* (1), 134–148.
- (20) Renier, C.; Pao, E.; Che, J.; Liu, H. E.; Lemaire, C. A.; Matsumoto, M.; Triboulet, M.; Srivinas, S.; Jeffrey, S. S.; Rettig, M.; Kulkarni, R. P.; Di Carlo, D.; Sollier-Christen, E. Label-Free Isolation of Prostate Circulating Tumor Cells Using Vortex Microfluidic Technology. *Npj Precis. Oncol.* **2017**, *1* (1), 1–11.
- (21) Armbrrecht, L.; Rutschmann, O.; Szczerba, B. M.; Nikoloff, J.; Aceto, N.; Dittrich, P. S. Quantification of Protein Secretion from Circulating Tumor Cells in Microfluidic Chambers. *Adv. Sci.* **2020**, *7* (11), 1903237.
- (22) Sivaramakrishnan, M.; Kothandan, R.; Govindarajan, D. K.; Meganathan, Y.; Kandaswamy, K. Active Microfluidic Systems for Cell Sorting and Separation. *Curr. Opin. Biomed. Eng.* **2020**, *13*, 60–68.
- (23) Mohammadi, R.; Asghari, M.; Colombo, M.; Vaezi, Z.; Richards, D. A.; Stavrakis, S.; Naderi-Manesh, H.; deMello, A. Hybrid Microfluidic Device for High Throughput Isolation of Cells Using Aptamer Functionalized Diatom Frustules. *CHIMIA* **2022**, *76* (7–8), 661–668.
- (24) Bidard, F. C.; Peeters, D. J.; Fehm, T.; Nolè, F.; Gisbert-Criado, R.; Mavroudis, D.; Grisanti, S.; Generali, D.; Garcia-Saenz, J. A.; Stebbing, J.; Caldas, C.; Gazzaniga, P.; Manso, L.; Zamarchi, R.; Lascoiti, A. F.; deDe Mattos-Arruda, L.; Ignatiadis, M.; Lebofsky, R.; Laere, S. J.; vanMeier-Stiegen, F.; Sandri, M. T.; Vidal-Martinez, J.; Politaki, E.; Consoli, F.; Bottini, A.; Diaz-Rubio, E.; Krell, J.; Dawson, S.-J.; Raimondi, C.; Rutten, A.; Janni, W.; Munzone, E.; Carañana, V.; Agelaki, S.; Almici, C.; Dirix, L.; Solomayer, E. F.; Zorzino, L.; Johannes, H.; Reis-Filho, J. S.; Pantel, K.; Pierga, J. Y.; Michiels, S. Clinical Validity of Circulating Tumour Cells in Patients with Metastatic Breast Cancer: A Pooled Analysis of Individual Patient Data. *Lancet Oncol.* **2014**, *15* (4), 406–414.
- (25) Gorges, T. M.; Tinhofer, I.; Drosch, M.; Röse, L.; Zollner, T. M.; Krahn, T.; von Ahsen, O. Circulating Tumour Cells Escape from EpCAM-Based Detection Due to Epithelial-to-Mesenchymal Transition. *BMC Cancer* **2012**, *12* (1), 178.
- (26) Schiro, P. G.; Zhao, M.; Kuo, J. S.; Koehler, K. M.; Sabath, D. E.; Chiu, D. T. Sensitive and High-Throughput Isolation of Rare Cells from Peripheral Blood with Ensemble-Decision Aliquot Ranking. *Angew. Chem., Int. Ed. Engl.* **2012**, *51* (19), 4618–4622.
- (27) Yang, J.; Weinberg, R. A. Epithelial-Mesenchymal Transition: At the Crossroads of Development and Tumor Metastasis. *Dev. Cell* **2008**, *14* (6), 818–829.
- (28) Sieuwerts, A. M.; Kraan, J.; Bolt, J.; Spoel, P.; van der Elstrodt, F.; Schutte, M.; Martens, J. W.; Gratama, J. W.; Sleijfer, S.; Foekens, J. A. Anti-Epithelial Cell Adhesion Molecule Antibodies and the Detection of Circulating Normal-Like Breast Tumor Cells. *J. Natl. Cancer Inst.* **2009**, *101* (1), 61–66.

- (29) Gross, H. J.; Verwer, B.; Houck, D.; Hoffman, R. A.; Recktenwald, D. Model Study Detecting Breast Cancer Cells in Peripheral Blood Mononuclear Cells at Frequencies as Low as 10^{-7} . *Proc. Natl. Acad. Sci.* **1995**, *92* (2), 537–541.
- (30) Ma, Z.; Zhou, Y.; Collins, J.; Ai, Y. Fluorescence Activated Cell Sorting via a Focused Traveling Surface Acoustic Beam. *Lab. Chip* **2017**, *17* (18), 3176–3185.
- (31) Perfetto, S. P.; Ambrozak, D. R.; Koup, R. A.; Roederer, M. Measuring Containment of Viable Infectious Cell Sorting in High-Velocity Cell Sorters. *Cytometry, Part A* **2003**, *52A* (2), 122–130.
- (32) Holmes, K. L.; Fontes, B.; Hogarth, P.; Konz, R.; Monard, S.; Pletcher, C. H.; Jr. Wadley, R. B.; Schmid, I.; Perfetto, S. P. International Society for the Advancement of Cytometry Cell Sorter Biosafety Standards. *Cytometry, Part A* **2014**, *85* (5), 434–453.
- (33) Ren, L.; Yang, S.; Zhang, P.; Qu, Z.; Mao, Z.; Huang, P. H.; Chen, Y.; Wu, M.; Wang, L.; Li, P.; Huang, T. J. Standing Surface Acoustic Wave (SSAW)-Based Fluorescence-Activated Cell Sorter. *Small* **2018**, *14* (40), 1801996.
- (34) Baret, J. C.; Miller, O. J.; Taly, V.; Ryckelynck, M.; El-Harrak, A.; Frenz, L.; Rick, C.; Samuels, M. L.; Hutchison, J. B.; Agresti, J. J.; Link, D. R.; Weitz, D. A.; Griffiths, A. D. Fluorescence-Activated Droplet Sorting (FADS): Efficient Microfluidic Cell Sorting Based on Enzymatic Activity. *Lab. Chip* **2009**, *9* (13), 1850–1858.
- (35) Neun, S.; Brear, P.; Campbell, E.; Tryfona, T.; El Omari, K.; Wagner, A.; Dupree, P.; Hyvönen, M.; Hollfelder, F. Functional Metagenomic Screening Identifies an Unexpected β -Glucuronidase. *Nat. Chem. Biol.* **2022**, *18* (10), 1096–1103.
- (36) Lee, D.; Hwang, B.; Kim, B. The Potential of a Dielectrophoresis Activated Cell Sorter (DACS) as a next Generation Cell Sorter. *Micro Nano Syst. Lett.* **2016**, *4* (1), 2.
- (37) Wang, X.; Chen, S.; Kong, M.; Wang, Z.; Costa, K. D.; Li, R.; Sun, D. Enhanced Cell Sorting and Manipulation with Combined Optical Tweezer and Microfluidic Chip Technologies. *Lab. Chip* **2011**, *11* (21), 3656–3662.
- (38) Landenberger, B.; Höfemann, H.; Wadle, S.; Rohrbach, A. Microfluidic Sorting of Arbitrary Cells with Dynamic Optical Tweezers. *Lab. Chip* **2012**, *12* (17), 3177–3183.
- (39) McIlvenna, D.; Huang, W. E.; Davison, P.; Glidle, A.; Cooper, J.; Yin, H. Continuous Cell Sorting in a Flow Based on Single Cell Resonance Raman Spectra. *Lab. Chip* **2016**, *16* (8), 1420–1429.
- (40) Wu, M.; Huang, P.-H.; Zhang, R.; Mao, Z.; Chen, C.; Kemeny, G.; Li, P.; Lee, A. V.; Gyanchandani, R.; Armstrong, A. J.; Dao, M.; Suresh, S.; Huang, T. J. Circulating Tumor Cell Phenotyping via High-Throughput Acoustic Separation. *Small* **2018**, *14* (32), 1801131.
- (41) Jiao, Z.; Han, Y.; Zhao, J.; Chao, Z.; Tárnok, A.; You, Z. Rapid Switching and Durable On-Chip Spark-Cavitation-Bubble Cell Sorter. *Microsyst. Nanoeng.* **2022**, *8* (1), 1–10.
- (42) Schiro, P. G.; Gadd, J. C.; Yen, G. S.; Chiu, D. T. High-Throughput Fluorescence-Activated Nanoscale Subcellular Sorter with Single-Molecule Sensitivity. *J. Phys. Chem. B* **2012**, *116* (35), 10490–10495.
- (43) Zhao, M.; Nelson, W. C.; Wei, B.; Schiro, P. G.; Hakimi, B. M.; Johnson, E. S.; Anand, R. K.; Gyurkey, G. S.; White, L. M.; Whiting, S. H.; Coveler, A. L.; Chiu, D. T. New Generation of Ensemble-Decision Aliquot Ranking Based on Simplified Microfluidic Components for Large-Capacity Trapping of Circulating Tumor Cells. *Anal. Chem.* **2013**, *85* (20), 9671–9677.
- (44) Zhao, M.; Wei, B.; Nelson, W. C.; Schiro, P. G.; Chiu, D. T. Simultaneous and Selective Isolation of Multiple Subpopulations of Rare Cells from Peripheral Blood Using Ensemble-Decision Aliquot Ranking (eDAR). *Lab. Chip* **2015**, *15* (16), 3391–3396.
- (45) Johnson, E. S.; Anand, R. K.; Chiu, D. T. Improved Detection by Ensemble-Decision Aliquot Ranking of Circulating Tumor Cells with Low Numbers of a Targeted Surface Antigen. *Anal. Chem.* **2015**, *87* (18), 9389–9395.
- (46) Sharma, S.; Zhuang, R.; Long, M.; Pavlovic, M.; Kang, Y.; Ilyas, A.; Asghar, W. Circulating Tumor Cell Isolation, Culture, and Downstream Molecular Analysis. *Biotechnol. Adv.* **2018**, *36* (4), 1063–1078.
- (47) Hao, S. J.; Wan, Y.; Xia, Y. Q.; Zou, X.; Zheng, S. Y. Size-Based Separation Methods of Circulating Tumor Cells. *Adv. Drug Delivery Rev.* **2018**, *125*, 3–20.
- (48) Xu, S.; Wu, L.; Qin, Y.; Jiang, Y.; Sun, K.; Holcomb, C.; Gravett, M. G.; Vojtech, L.; Schiro, P. G.; Chiu, D. T. Sequential Ensemble-Decision Aliquot Ranking Isolation and Fluorescence In Situ Hybridization Identification of Rare Cells from Blood by Using Concentrated Peripheral Blood Mononuclear Cells. *Anal. Chem.* **2021**, *93* (6), 3196–3201.
- (49) Holzner, G.; Mateescu, B.; van Leeuwen, D.; Cereghetti, G.; Dechant, R.; Stavakis, S.; deMello, A. High-Throughput Multiparametric Imaging Flow Cytometry: Toward Diffraction-Limited Sub-Cellular Detection and Monitoring of Sub-Cellular Processes. *Cell Rep.* **2021**, *34* (10), No. 108824.
- (50) Aslan, M. K.; Meng, Y.; Zhang, Y.; Weiss, T.; Stavakis, S.; deMello, A. J. Ultrahigh-Throughput, Real-Time Flow Cytometry for Rare Cell Quantification from Whole Blood. *ACS Sens.* **2024**, *9* (1), 474–482.
- (51) Holzner, G.; Stavakis, S.; deMello, A. Elasto-Inertial Focusing of Mammalian Cells and Bacteria Using Low Molecular, Low Viscosity PEO Solutions. *Anal. Chem.* **2017**, *89* (21), 11653–11663.
- (52) Vertti-Quintero, N.; Berger, S.; Casadevall I Solvas, X.; Statzer, C.; Annis, J.; Ruppen, P.; Stavakis, S.; Ewald, C. Y.; Gunawan, R.; deMello, A. J. Stochastic and Age-Dependent Proteostasis Decline Underlies Heterogeneity in Heat-Shock Response Dynamics. *Small* **2021**, *17* (30), No. 2102145.
- (53) Okahara, K.; Sun, B.; Kambayashi, J. Upregulation of Prostacyclin Synthesis-Related Gene Expression by Shear Stress in Vascular Endothelial Cells. *Arterioscler., Thromb., Vasc. Biol.* **1998**, *18* (12), 1922–1926.
- (54) Wernig, F.; Mayr, M.; Xu, Q. Mechanical Stretch-Induced Apoptosis in Smooth Muscle Cells Is Mediated by B1-Integrin Signaling Pathways. *Hypertension* **2003**, *41* (4), 903–911.
- (55) Visal, T. H.; den Hollander, P.; Cristofanilli, M.; Mani, S. A. Circulating Tumour Cells in the -Omics Era: How Far Are We from Achieving the ‘Singularity’? *Br. J. Cancer* **2022**, *127* (2), 173–184.
- (56) Vijayakumar, K.; Gulati, S.; deMello, A. J.; Edel, J. B. Rapid Cell Extraction in Aqueous Two-Phase Microdroplet Systems. *Chem. Sci.* **2010**, *1* (4), 447–452.